Photocatalytic Degradation of (Neomycin) Antibiotic Concentrated Pharmaceutical Disposals using *Ficus hispida* Synthesized Fe Nanoparticles under Simulated Sunlight

Mathivanan Varatharajan[1], Murugesan Kumarasamy[2]*, Siddharth Sampathkumar[2]

[1]Department of Environmental Science, Periyar University, Periyar Palkalai Nagar, Salem - 636011, Tamil Nadu, India
[2]Department of Mechanical Engineering, PSN College of Engineering & Technology, PSN Nagar, PSN College Rd, Melathediyoor, Tirunelveli, Tamil Nadu 627152
Corresponding author: kmurugesan@gmail.com

Abstract

In recent times, the presence of aminoglycoside antibiotic waste in water bodies and the environment has become a serious issue. To address this, it is important to reduce the toxicity of antibiotics in pharmaceutical waste management. In this study, the photo-catalytic degradation of the aminoglycoside antibiotic neomycin using Fe Nano Particles (NPs) synthesized from *Ficus hispida* has been investigated. For the synthesis of Fe NPs, Fe (II) sulphate salt (FeSO4•7H2O) was used and treated with *Ficus hispida* extract to prepare biosynthesized Fe NPs. Alternatively, chemically synthesized Fe NPs were prepared using sodium borohydride. The degradation efficiency of *Ficus hispida* synthesized Fe NPs was 3.1 times greater than that of chemically synthesized Fe NPs in the photo-catalytic degradation of neomycin-rich pharmaceutical waste water. This improvement was attributed to the greater surface area of *Ficus hispida* synthesized Fe NPs ($6.3 \ m^2/g$) compared to chemically synthesized Fe NPs ($4.8 \ m^2/g$). The degradation kinetics were evaluated using the Langmuir–Hinshelwood model and the importance of surface reactions in improving the photo-catalytic reactions were ascertained. Piperidine and piperazine immobilization on *Ficus hispida* synthesized Fe NPs and chemically synthesized Fe NPs increased neomycin antibiotic degradation. Antibiotic activity experiments were conducted on the treated residues and the results indicated that *Ficus hispida* synthesized Fe NPs were more effective than chemically synthesized Fe NPs.

Keywords: *Ficus hispda*, Fe nanoparticles, antibiotic wastes, neomycin, photo catalytic degradation

Introduction

In recent times, it was observed that around 20 to 25% of antibiotics go unused and are dumped in the environment as pharmaceutical and medical waste effluents. The release of such antibiotic infused waste in the environment causes pollution and it affects biodiversity (1). Pharmaceutical effluents in the environment are undesirable, as they become toxic and affect the health of human beings. They tend to make the drinking water poisonous and pollute the regions in which they are dumped. Such pharmaceutical wastes dumped in the environment also affect marine life and microorganisms (2). Marine sponges in coral reefs such

as *Ircinia fusca* by themselves possess antibiotic properties. Dumping of wastes affects the marine aqua system and forms fish pathogens (3). Lack of clean and pure water has become a global challenge due to the continuous increase in human population. A lot of studies have indicated the presence of antibiotics in water in dangerously large quantities (4). Consumption of pharmaceutical compounds infused drinking water causes a lot of diseases in human beings. The presence of *Ocimum basillicum* in soils had a toxic effect on the plants grown in that area and affected the photosynthesis process of the plants (5). Even though there are sewage treatment plants and detoxification equipment, these are not fully adequate for removing complex pollutants and antibiotics.

There is a need for pursuing research in developing innovative methods to detoxify and degrade the pollutants which have greater chemical stability. Isolation of biofilm-producing bacteria from a treatment tank (6), Photolysis, ozonation (7), ultrasound radiation (8), electrochemical oxidation (9), sonolysis and fungal biodegradation (10) are some of the oxidation methods used for wastewater treatment.

Biopharmaceutical and medical wastewater consist of antibiotics in high concentrations. It exhibits high chemical toxicity and undesirably large levels of salt content. Biological treatment is important for removing the organic pollutants and advanced treatment is necessary for removing the antibiotics mixed in waste water. Out of the different methods, photo-catalysis is the renowned process for degrading organic pollutants (11). Generally, during photo-catalysis process, the usage of visible light is low and the rate of charge recombination is very high (12). During photo-catalytic activity, oxygen rich radicals present on the surface affect the degradation rate (13).

Use of Nano Particles (NPs) for wastewater treatment has increased in recent times (14). Out of different based NPs, Fe NPs are found to be economical compared to titanium and silver based NPs (15). For preparing Fe and Fe-based NPs, different synthesis routes are being used. Biosynthesis method for preparing NPs an easy method and it exhibits better degradation ability (16), compared to other chemically synthesized NPs. Plant extracts and leaf extracts are being used for synthesis of Fe based NPs (17). Compared to biosynthesis process for preparing metal NPs, chemical and physical methods were found to be costly (18). The overall time taken for the synthesis of NPs using biosynthesis process was found to be less, compared to chemical and physical synthesis processes. Extensive research has been conducted to identify the biocompatibility of the synthesized Fe based NPs in toxin reduction.

Azacycloalkanes such as piperidine and piperazines act as precursors for many bio-active reactions (19). During bio-degradation studies, the presence of piperidine and piperazines helped in modifying the bioconversion kinetics favorably (20). They help in reducing the inhibition developed during chemical activity (21) and preventing the formation of resistive intermediates. They help in improving the reaction rate without compromising the reactants (22). Piperidine immobilization helped in improving multi-component reactions (23) and increased magnetically retrievably capability of α-Fe_2O_3 (24). It acts as a catalyst for organic synthesis. Piperazine acts as a heterogeneous bi-functional catalyst (25). Immobilization using piperazine increases the stability of the reaction (26). The linear intermediates developed during chemical reactions are supported using piperazine linkers (27). In nano-filtration using thin film composite membranes, piperazine immobilization of monomers improves co-deposition and stability of the deposited monomers (28).

Characteristics of the prepared metal-based NPs were done using ultraviolet-visible (UV-Vis) spectroscopy (29), Fourier Transform Infrared ray Spectroscopy (FTIR), X-Ray diffraction studies (XR-D) (30) and Scanning Electron Microscopy (SEM).

Photocatalytic degradation of (neomycin) antibiotic concentrated pharmaceutical disposals using *Ficus hispida* synthesized fe nanoparticels under simulated sunlight

In this investigation, degradation of neomycin rich pharmaceutical waste water was done by using Fe based NPs synthesized by using *Ficus hispida* extract and chemical synthesis. The prepared Fe NPs were subjected to piperidine and piperazine immobilization and an improvement in degradation rate was observed. Residual antibacterial activity studies were conducted to find the balance antibiotic content in the waste water.

Materials & Methods

Chemicals used

For conducting experiments, the following chemicals such as ferrous sulphate heptahydrate, sodium boro hydroxide, sodium hydroxide, 3-Chloropropyl-trimethoxysilane, hydrochloric acid, piperidine, piperazine and-de-ionized water were purchased from Aksar Chemicals Pvt. Ltd. As the procured materials were 99.9% pure, they were used without any further purification. The beakers, funnels and other chemical processing equipment were washed with hydrochloric acid and dried.

Synthesis of Fe nanoparticles

Ficus hispida leaves were procured, dried and powdered using grinder. For preparing *Ficus hispida* extract, 5 g of powdered *Ficus hispida* was agitated in de-ionized water for 30 minutes at 90°C. Then, it was allowed to cool and it was filtered by using Whatman filter paper for removing larger impurities. The filtered *Ficus hispida* extract was centrifuged for 20 minutes. After centrifuging, it was made to pass through Millipore filter. Fe (II) sulphate salt ($FeSO_4.7H_2O$) solution was prepared at 0.005M concentration. At 4:1 ratio, *Ficus hispida* extract was mixed with Fe (II) sulphate salt solution using magnetic stirrer. Bio-synthesized Fe NPs were synthesized at room temperature (31). The prepared Fe NPs were washed with de-ionized water and ethanol for three times and then dried in a flask oven at 80°C. For preparing chemically synthesized Fe NPs, 0.6668 g of ferrous sulphate heptahydrate was added to 1.104 g of sodium borohydride

in 80 ml of de-ionized water and stirred till the substances were completely dissolved. The pH of the solution was maintained at 6 during the entire duration. After the substances were completely dissolved, its temperature was brought down to near-freezing temperature and then stirred vigorously at 1500 rpm. Chemical synthesis of Fe NPs was done at ambient temperature. For separating the prepared chemically synthesized Fe NPs, they were centrifuged at 6000 rpm for 15 minutes and separated using neodymium magnets. It was then filtered and dried in a vacuum for 10 hrs. *Ficus Hispida* synthesized Fe NPs and chemically synthesized Fe NPs were stored in ambient conditions for preventing contamination. *Ficus hispida* synthesized Fe NPs and chemically synthesized Fe NPs were subjected to piperidine and piperazine immobilization. For achieving this, the NPs were subjected to chloro-functionalization. 1.5 g of synthesized Fe NPs were mixed in 35 ml of toluene. 0.75 ml of 3-Chloropropyl-trimethoxysilane was added to it and the solution was heated to 100°C, by increasing the temperature gradually. The resulting chloro-functionalized Fe NPs were separated using neodymium magnets and then it was washed in diethyl ether. Drying of the chloro-functionalized Fe NPs was done in a vacuum. 0.05 g of piperidine was added to chloro-functionalized Fe NPs (0.9 g) in 15 ml toluene. Piperidine and NPs were stirred for 6 hrs, at very slow rpm. Then the resulting piperidine immobilized Fe NPs were washed in diethyl ether and then with CH_2Cl_2. After washing it, in both solutions, it was dried in a vacuum. A similar procedure was adopted for preparing piperamine immobilized Fe NPs.

Characterization of Fe NPs

The synthesized FeNPs were characterized by using Ultra Violet-Visible Spectroscopy testing equipment (UV-Vis spectroscopy). Test samples were prepared by centrifuging the NPs at 3800 rpm for 15 minutes. Then it was placed in the equipment and on transmitting light, the absorbance spectrum was analyzed. Using the nitrogen adsorption technique, at

1281

cryogenic temperatures (around 75 K), the surface area of the prepared Fe NPs was identified. Specific surface area studies were conducted by using Micromeritics ASAP equipment. The specific surface area was evaluated according to Barrett–Joyner–Halenda model of adsorption. Using X-Ray diffraction (X-RD) spectroscopy, the chemical aspects of the prepared NPs were studied. (RIGAKU-Make) X-RD equipment was used for conducting the experiments. From 20° to 80° two theta, using continuous scan, with step size of 0.005, Cu target, K alpha as 1.54 A°, X-RD experiments were conducted. The NPs were subjected to Fourier Transform Infrared Spectroscopy (FTIR) evaluation using (TOSHIN-Make) equipment. Electron spin resonance (ESR) studies were conducted on the prepared Fe NPs using Electron Spin Resonance Spectrometer (JEOL-Make).

Photo-catalytic detoxification of antibiotic wastes using the prepared Fe NPs

Detoxification studies were conducted using batch experiments (32). Prior to the conduct of the batch experiments, the beakers were sterilized. 25 ml of neomycin rich pharmaceutical waste water was mixed with Fe NPs. Agitation was done using ultrasonicator for half an hour. By recording the residual antibiotic activity, the effectiveness of the NPs was identified. Batch experiments were conducted by using *Ficus hispida* synthesized Fe Nps, piperidine immobilized *Ficus hispida* synthesized Fe NPs, piperazine immobilized *Ficus hispida* synthesized NPs, chemically synthesized Fe NPs, piperidine immobilized chemically synthesized Fe NPs and piperazine immobilized chemically synthesized Fe NPs (33). For all degradation experiments, the quantity of Fe NPs were 3 g/l, initial concentration of neomycin as 200 mg/l, reaction duration as 2 hrs, pH of the degradation batch as 8 and concentration of NaCl at 0.05M.

Residual antibiotic activity experiments

The residual antibiotic activity experiments were conducted to identify the detoxification efficiency of the prepared Fe NPs. It was observed by measuring the inhibition halo prepared around agar plate discs. 1.5×10^8 CUF/mL clostridium was inoculated on agar plates and parallel 10 µL reaction samples were planted on agar plates. At 37°C, with 1-day incubation, an increase in inhibition halo was evaluated.

Results & Discussion

Characterization of Fe NPs

The UV-Vis results of the characterized Fe NPs are shown in Fig. 1. UV-Vis graph of the non-aromatic and flexible piperidine is shown in Fig. 1(a). Absorbance peaks were identified at 204.65 nm. UV-Vis graph of piperazine (an azacycloalkane) is shown in Fig. 1(b). At 331.41 nm, an absorbance peak was found. Fig. 1(c) shows the UV-Vis graph of piperidine immobilized chemically synthesized Fe NPs. Absorbance peaks were observed at 339.23 nm. Fig. 1(d) shows the UV-Vis graph of piperazine immobilized chemically synthesized Fe NPs. Absorbance peaks were observed at 313.26 nm and 413.4 nm. Fig. 1(e) shows UV-Vis graph of piperidine immobilized *Ficus hispida* synthesized Fe NPs. The absorbance peak was identified at 276.39 nm. Fig. 1(f) shows UV-Vis graph of piperazine immobilized *Ficus hispida* synthesized Fe NPs and at 211.3 nm, 276.83 nm, absorbance peaks were found.

Fourier transform infrared spectroscopy (FTIR) results of the prepared NPs are shown in Fig. 2. Fig. 2(a) shows FTIR graph of piperidine. Near 3329 cm^{-1} shows stretching of N-H and 3289.1 cm^{-1} indicates C-C stretching. From 1450 cm^{-1} to 780 cm^{-1} stretching of C-N bond can be observed. FTIR spectrum of piperazine is shown in Fig. 2 (b). Near 835 cm^{-1}, stretching of C-Cl band was observed. Near 1642 cm^{-1}, reduction of C-Cl bond and amine such as N-H was observed. FTIR spectrum of piperidine immobilized chemically synthesized Fe NPs is shown in Fig. 2(c). A significant broadening of wavelength was identified from 535.4 cm^{-1} to 667.5 cm^{-1} indicating Fe-O vibrations. Fig. 2(d) shows the FTIR spectrum of piperazine immobi-
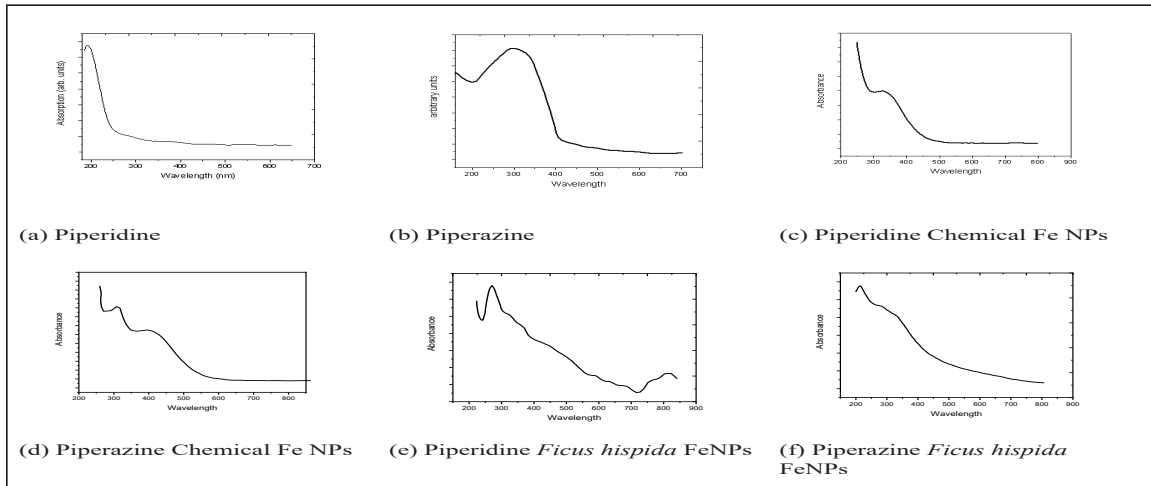
Fig. 1. UV-Vis spectroscopy results

lized chemically synthesized Fe NPs. C-H vibrations and stretch of alkyl chains were identified near 2963 cm^{-1}. A steep absorption was identified near 3473 cm^{-1} indicating N-H stretching. Fig. 2(e) shows the FTIR spectrum of piperidine immobilized *Ficus hispida* synthesized Fe NPs. Near 611.3 cm^{-1}, stretching of Fe-O vibration band was observed. The band identified near 2059.63 cm^{-1} shows –OH stretching. Presence of H bond was confirmed. FTIR spectrum of piperazine immobilized Ficus hispida synthesized Fe NPs are shown in Fig. 2(f). Absorption band near 1641.2 cm^{-1} indicates stretching of C=C.
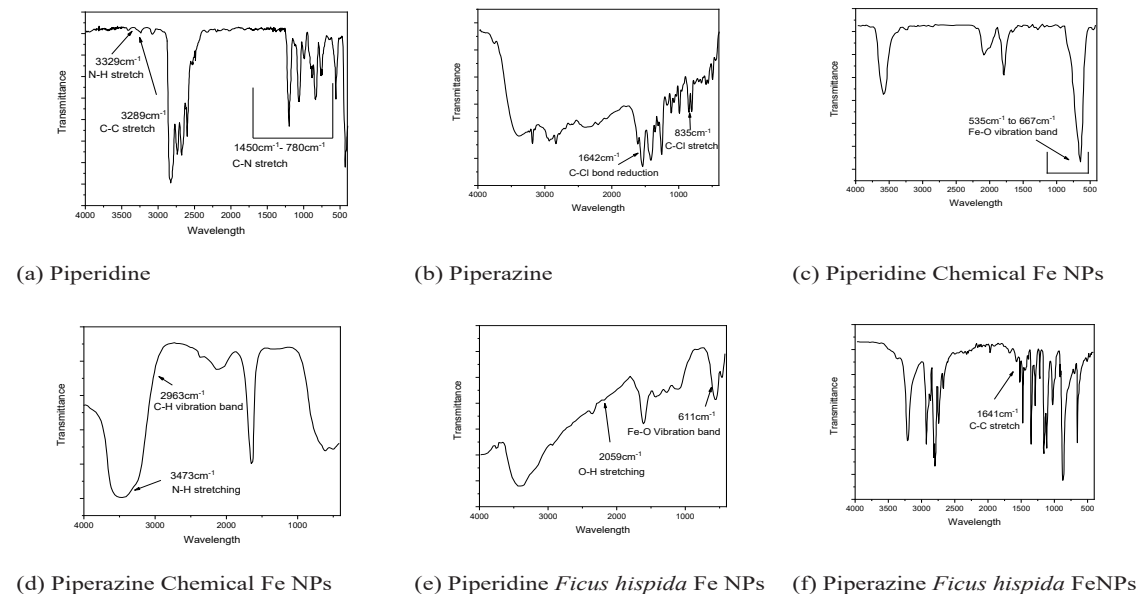

Fig. 2. FT-IR spectroscopy results

X-RD graphs of the chemicals and Fe NPs are shown in Fig. 3. Fig. 3 (a) shows the X-RD spectra for piperidine. Peaks were observed at 23.69º, 28.76º, 38.41º, 42.32º, 44.31º, 47.34º, 51.29º, 54.32º and 59.4º two theta. Fig. 3 (b) shows the X-RD spectra of piperazine. Peaks were observed at 23.14º, 32.14º, 43.21º, 52.14º and 66.49º two theta. Fig. 3 (c) shows the X-RD spectra for piperidine immobilized chemically synthesized Fe NPs. Peaks were found at 31.24º, 38.42º, 46.32º, 57.41º, 59.84º and 63.41º two theta. Fig. 3 (d) shows the X-RD spectra for piperazine immobilized chemically synthesized Fe NPs. Peaks were identified at 24.41°, 42.12°, 44.69°, 52.41°, 62.14° and 68.63° two theta. Fig. 3 (e) shows X-RD spectra for piperidine immobilized *Ficus hispida* synthesized Fe NPs. Peaks were identified 24.21°, 43.15°, 52.43°, 69.41° two theta. Figure 3 (f) shows the X-RD spectra for piperazine immobilized *Ficus hispida* synthesized Fe NPs and the corresponding two theta peaks were identified at 29.41°, 36.32°, 42.74°, 52.69°, 58.43° and 62.57°. α-Fe particles were identified near 44.69° two theta values (34). Compared to pip-

erazine immobilized *Ficus hispida* synthesized Fe NPs, piperidine immobilized *Ficus hispida* synthesized Fe NPs were found to be amorphous as the quantity of distinctive peaks were relatively low. The peaks identified near 24.21° were identified as organic materials from *Ficus hispida.*

Scanning Electron Microscopic (SEM) evaluation with EDAX (Energy Dispersive X-Ray Analysis) of Fe NPs is shown in Fig. 4. SEM with EDAX images of chemically synthesized Fe NPs, *Ficus hispida* synthesized Fe NPs, piperidine immobilized chemically synthesized Fe NPs, piperazine immobilized chemically synthesized Fe NPS, piperidine immobilized *Ficus hispida* synthesized Fe NPs and piperazine immobilized *Ficus hispida* synthesized Fe NPs are shown in Fig. 4 (a), (b), (c), (d) & (e) respectively. Chemically synthesized Fe NPs were found to round in shape. Both chemically synthesized Fe NPs and *Ficus hispida* synthesized Fe NPs were ultrafine. Synthesis of *Ficus hispida* synthesized Fe NPs was done at 90°C, contrary to the chemical synthesis method in which syn-
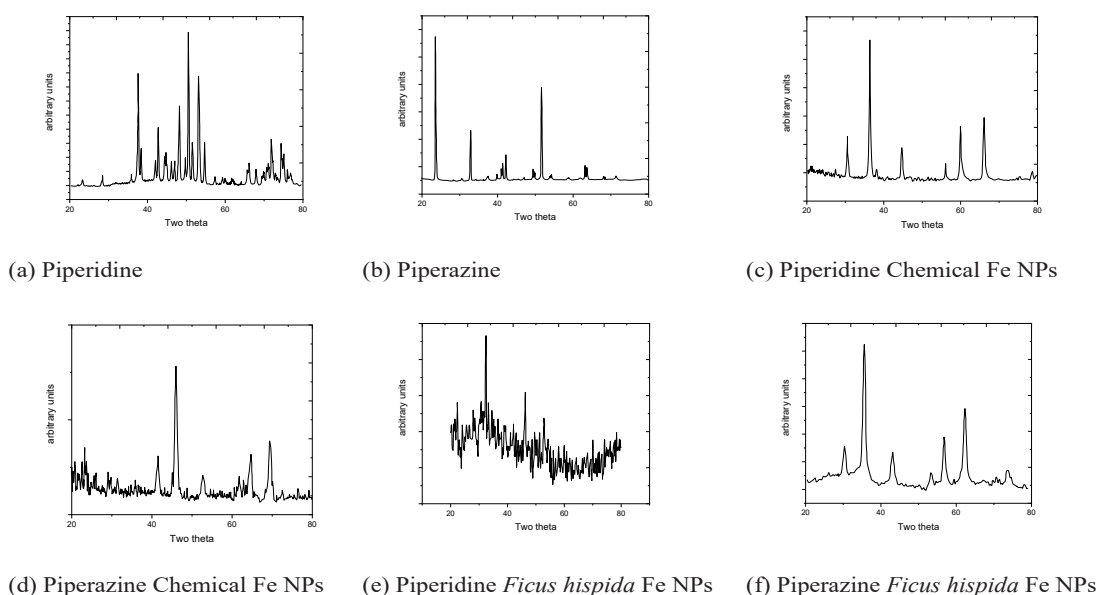

(a) Piperidine

(b) Piperazine

(c) Piperidine Chemical Fe NPs

(d) Piperazine Chemical Fe NPs

(e) Piperidine *Ficus hispida* Fe NPs

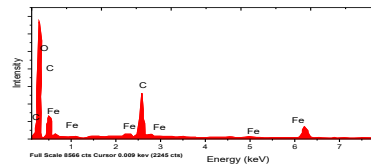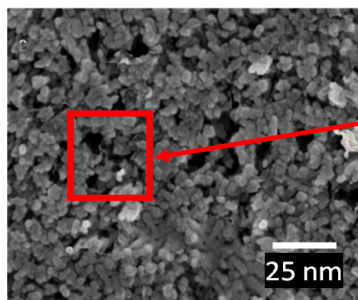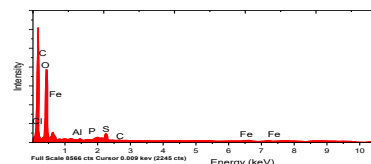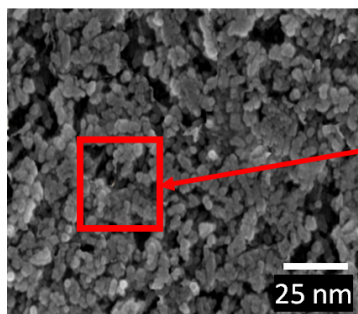(f) Piperazine *Ficus hispida* Fe NPs

Fig. 3. X-RD results

Photocatalytic degradation of (neomycin) antibiotic concentrated pharmaceutical disposals using *Ficus hispida* synthesized fe nanoparticels under simulated sunlight

thesis was done near freezing temperature. An increase in overall size of the *Ficus hispida* synthesized Fe NPs was observed by comparing it to the overall size of the Fe NPs synthesized using chemical synthesis method. From UV-Vis spectroscopic evaluation, diminished peaks were observed for *Ficus hispida* synthesized Fe NPs. Fe NPs synthesized using plant extracts results in increased particle sizes (35). The reactivity of NPs is inversely proportional to its size. Hence, increase in the size of NPs results in reduced reactivity. During bio-synthesis of Fe NPs, agglomeration of reducing agents to the surface of preformed nuclei occurs. On nuclei surface, aggregation of reducing agents causes secondary reduction of Fe ions. This increased the growth rate of Fe NPs (36). The presence of Cl in piperidine and piperazine immobilized Fe NPs was observed. Quantitative analysis indicated that the ratio of O/Fe for Fe NPs varied from 1.165 to 1.612. Piperidine and piperazine immobilization resulted in increase of O/Fe atomic ratios were around 1.525, which was closer to the theoretical atomic ratios (O/Fe) of Iron oxides.
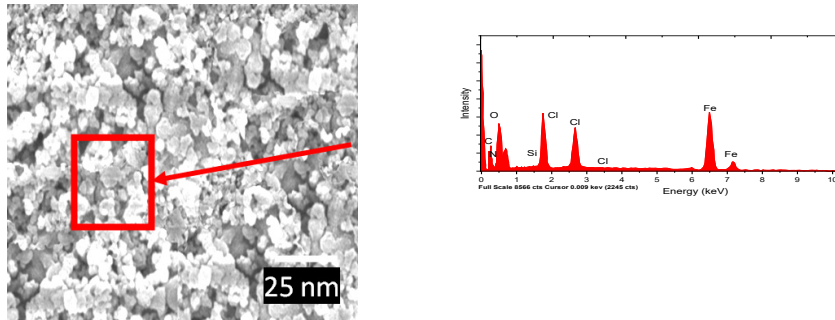

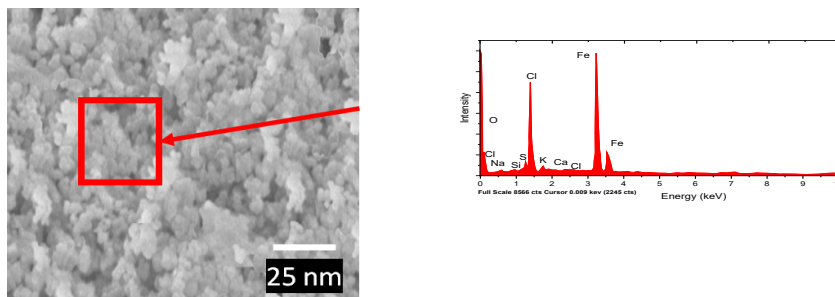(a) SEM - EDAX spectrum of chemically synthesized Fe NPs

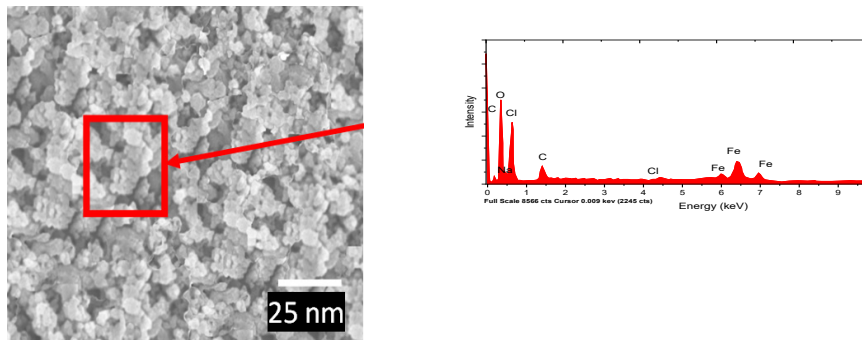(b) SEM - EDAX spectrum of *Ficus hispida* synthesized Fe NPs
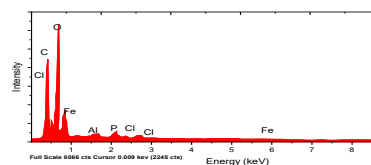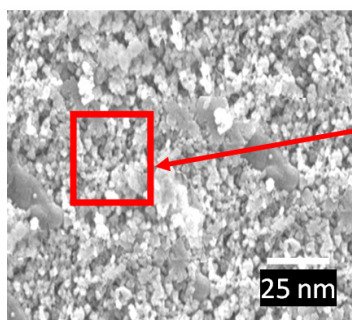
(c) SEM - EDAX spectrum of Piperidine immobilized chemically synthesized Fe NPs

(d) SEM - EDAX spectrum of Piperazine immobilized chemically synthesized Fe NPs

(e) SEM – EDAX spectrum of piperidine immobilized *Ficuhispida* synthesized Fe NPs

(f) SEM – EDAX spectrum of piperazine immobilized *Ficus hispida* synthesized Fe NPs

Fig. 4. FESEM images with EDAX spectrum of (a) Chemically synthesized Fe NPs, (b) *Ficus hispida* synthesized Fe NPs, (c) Piperidine immobilized Chemically synthesized Fe NPs, (d) Piperazine immobilized Chemically syntheisized Fe NPs, (e) Piperidine immobilized *Ficus hispida* synthesized Fe NPs, (f) Piperazine immobilized *Ficus hispida* synthesized Fe NPs.

Batch experiments

Batch experiments were conducted on neomycin rich pharmaceutical waste water under simulated sunlight environment (solar irradiance of 650-700 W/m^2) using Fe NPs. Prior to addition of the Fe NPs into the waste water, the pH of the solution was 4.1. On adding the

Fe NPs, an increase in pH of the solution was observed. On adding chemically synthesized Fe NPs, the pH of the solution increased to 7.2. On adding *Ficus hispida* synthesized Fe NPs, the pH of the solution increased to 6.8. Interaction of Fe NPs with the pharmaceutical waste water caused formation of hydroxyl ions. Antibiotic degradation was observed on adding Fe NPs. A considerable increase in antibiotic degradation was observed under photocatalytic degradation on immobilization of Fe NPs with piperidine and piperazine. In the absence of photocatalysis, no significant improvement in antibiotic degradation was found using piperidine and piperazine immobilization.

Reaction kinetics

Under simulated sunlight, the reaction kinetics of antibiotic degradation, under piperidine immobilized chemically synthesized Fe NPs, piperidine immobilized *Ficus hispida* synthesized Fe NPs, piperazine immobilized chemically synthesized Fe NPs and piperazine immobilized *Ficus hispida* synthesized Fe NPs were evaluated using Langmuir-Hinshelwood (LH) model (37). In suspension models, LH mechanism is used for evaluation of the photo-catalytic activity involved in it. A photo-catalytic reaction is termed to follow LH model when the relationship between the reaction rate of the activity and the reaction substrate concentration exhibits linear reciprocal association. The equation for reaction rate R_r is shown below

$$R_r = \frac{S_k \times L_s \times E_K \times C_s}{E_K \times C_s + 1}$$ Eq. 1

In the above equation, S_k is the rate constant of substrate subjected to adsorption at the surface of the reaction having $e^-(h^+)$, E_k is the adsorption constant at equilibrium condition, L_s is the surface adsorption's limiting factor and C_s is the substrate's concentration at equilibrium conditions. When substrate adsorption is witnessed during a photo-catalytic reaction obeying LH model, adsorption equilibrium is maintained throughout the degradation reaction. When the adsorption rate is quicker than the reaction with e^-_s and h^+_s, it is identified as

Light Intensity Limited (LIL) reaction. LIL reaction indicates that photo-adsorption determines reaction rate. For determining Langmuir-Hinshelwood (LH) kinetics, reciprocal rate vs reciprocal concentration and ratio of concentration to rate against concentration was identified. Figure 5 shows Langmuir-Hinshelwood kinetics plot of $1/R_r$ vs $1/C_s$. All degradation reactions were conducted under simulated sunlight (photo-catalytic environment). The variations were plotted and the best fit was chosen to plot the graph. The variations in $1/R_r$ vs $1/C_s$ for neomycin antibiotic degradation reaction using chemically synthesized Fe NPs under photo-catalytic environment is shown in Figure 5 (a). The equation for line is shown below and the coefficient of determination R^2 value for the line was identified as 0.8783.

$$y = 0.8179x + 4.2132$$ Eq. 2

The variations in $1/R_r$ vs $1/C_s$ for neomycin antibiotic degradation reaction using *Ficus hispida* synthesized Fe NPs under photo-catalytic environment is shown in Figure 5 (b). The equation for line is shown below and the coefficient of determination R^2 value for the line was identified as 0.8948.

$$y = 0.8521x + 4.6136$$ Eq. 3

The variations in $1/R_r$ vs $1/C_s$ for neomycin antibiotic degradation reaction using Piperidine immobilized chemically synthesized Fe NPs under photo-catalytic environment is shown in Figure 5 (c). The equation for line is shown below and the coefficient of determination R^2 value for the line was identified as 0.9124.

$$y = 0.8743x + 4.9429$$ Eq. 4

The variations in $1/R_r$ vs $1/C_s$ for neomycin antibiotic degradation reaction using Piperazine immobilized chemically synthesized Fe NPs under photo-catalytic environment is shown in Figure 5 (d). The equation for line is shown below and the coefficient of determination R^2 value for the line was identified as 0.9426.

$$y = 0.8932x + 5.1468 \qquad \text{Eq. 5}$$

The variations in $1/R_r$ vs $1/C_s$ for neomycin antibiotic degradation reaction using Piperidine immobilized *Ficus hispida* synthesized Fe NPs under photo-catalytic environment is shown in Figure 5 (e). The equation for line is shown below and the coefficient of determination R^2 value for the line was identified as 0.9512.

$$y = 0.9182x + 5.4389 \qquad \text{Eq. 6}$$

The variations in $1/R_r$ vs $1/C_s$ for neomycin antibiotic degradation reaction using Piperazine immobilized *Ficus hispida* synthesized Fe NPs under photo-catalytic environment is shown in Figure 5 (f). The equation for line is shown below and the coefficient of determination R^2 value for the line was identified as 0.9642.

(a) Chemical Fe NPs (b) *Ficus hispida* synthesized FeNPs (c) Piperidine Chemical Fe NPs

(d) Piperazine Chemical Fe NPs (e) Piperidine *Ficus hispida* Fe NPs (f) Piperazine *Ficus hispida* Fe NPs

Fig. 5. Langmuir-Hinshelwood kinetics plot of $1/R_r$ vs $1/C_s$.

$$y = 0.9236x + 5.8416 \qquad \text{Eq. 7}$$

Fig. 6 shows Langmuir-Hinshelwood kinetics plot of C_s/R_r vs C_s. The variations in C_s/R_r vs C_s for neomycin antibiotic degradation reaction using chemically synthesized Fe NPs under photo-catalytic environment is shown in Figure 6 (a). The equation for line is shown below and the coefficient of determination R^2 value for the line was identified as 0.8526
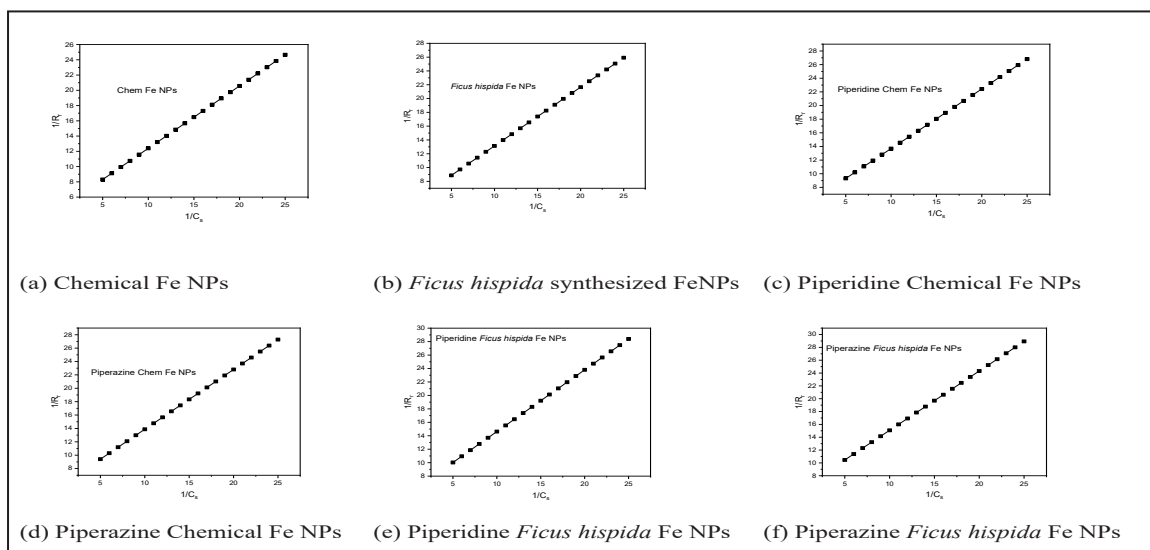
$$y = 0.7731x - 4.5149 \qquad \text{Eq. 8}$$

The variations in C_s/R_r vs C_s for neomycin antibiotic degradation reaction using *Ficus hispida* synthesized Fe NPs under photo-catalytic environment is shown in Figure 6 (b). The equation for line is shown below and the coeffi-

cient of determination R^2 value for the line was identified as 0.8639

$$y = 0.7943x - 4.4129 \qquad \text{Eq. 9}$$

The variations in C_s/R_r vs C_s for neomycin antibiotic degradation reaction using Piperidine immobilized chemically synthesized Fe NPs under photo-catalytic environment is shown in Figure 6 (c). The equation for line is shown below and the coefficient of determination R^2 value for the line was identified as 0.8741.

$$y = 0.8179x - 4.3124 \qquad \text{Eq. 10}$$

The variations in C_s/R_r vs C_s for neomycin antibiotic degradation reaction using Piperazine immobilized chemically synthesized Fe NPs under photo-catalytic environment is shown

Current Trends in Biotechnology and Pharmacy
Vol. 17(Supplementary issue - 3B) 1278-1292,September 2023, ISSN 0973-8916 (Print), 2230-7303 (Online)
10.5530/ctbp.2023.3s.63

1288

in Figure 6 (d). The equation for line is shown below and the coefficient of determination R^2 value for the line was identified as 0.8932.

$$y = 0.8232x - 4.1214 \qquad \text{Eq. 11}$$

The variations in C_s/R_r vs C_s for neomycin antibiotic degradation reaction using Piperidine immobilized *Ficus hispida* synthesized Fe NPs under photo-catalytic environment is shown in Figure 6 (e). The equation for line is shown below and the coefficient of determination R^2 value for the line was identified as 0.9012.

$$y = 0.8411x - 3.9217 \qquad \text{Eq. 12}$$

The variations in C_s/R_r vs C_s for neomycin antibiotic degradation reaction using Piperazine immobilized *Ficus hispida* synthesized Fe NPs under photo-catalytic environment is shown in Figure 6 (f). The equation for line is shown below and the coefficient of determination R^2 value for the line was identified as 0.9146.
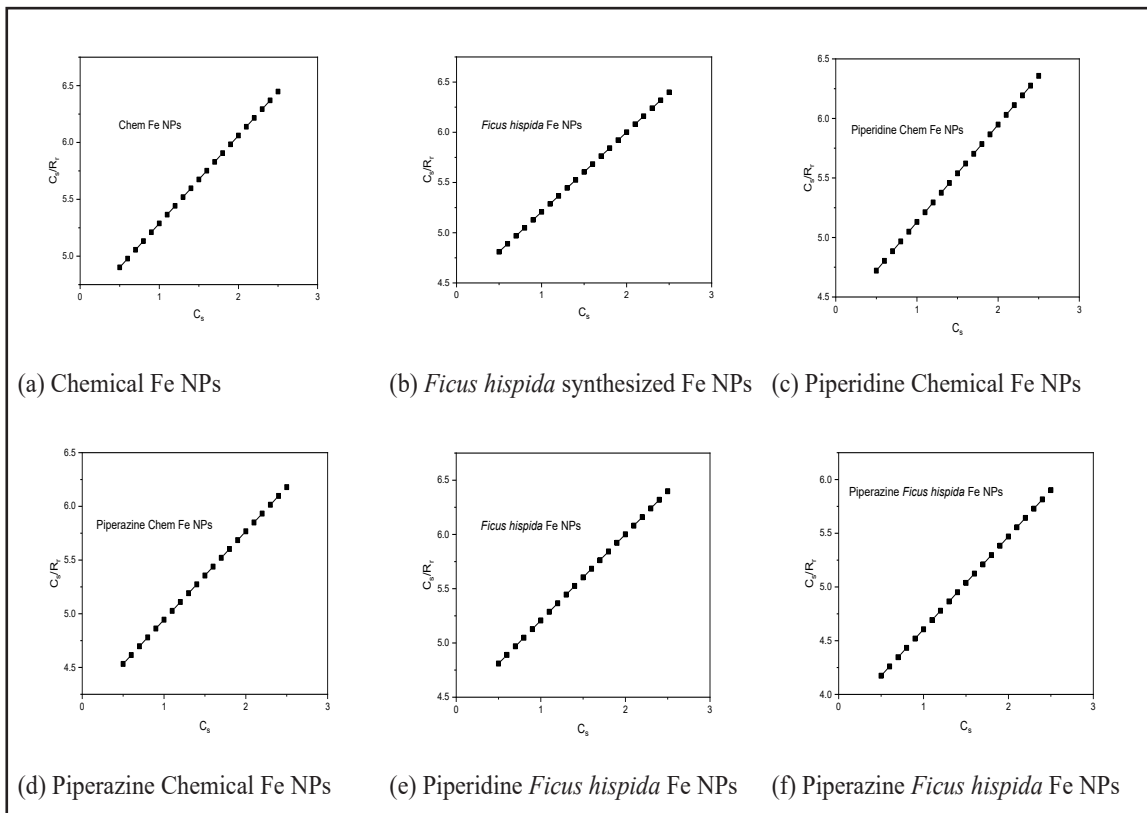
$$y = 0.8639x - 3.7419 \qquad \text{Eq. 13}$$

Fig. 6. Langmuir-Hinshelwood kinetics plots of C_s/R_r vs C_s

Langmuir-Hinshelwood kinetics mechanism involves the reaction between two types of molecules, which occurs on the surface. Adsorption of the molecules occurs in the same adsorption sites. For both plots of $1/R_r$ vs $1/C_s$. and C_s/R_r vs C_s, the value of R^2 was closer to unity on subjecting chemically synthesized Fe NPs and *Ficus hispida* synthesized Fe NPs to piperidine and piperazine immobilization.

The Electron Spin Resonance spectrum on evaluating the chemically synthesized nanoparticles with and without immobilization is shown in Fig. 7.
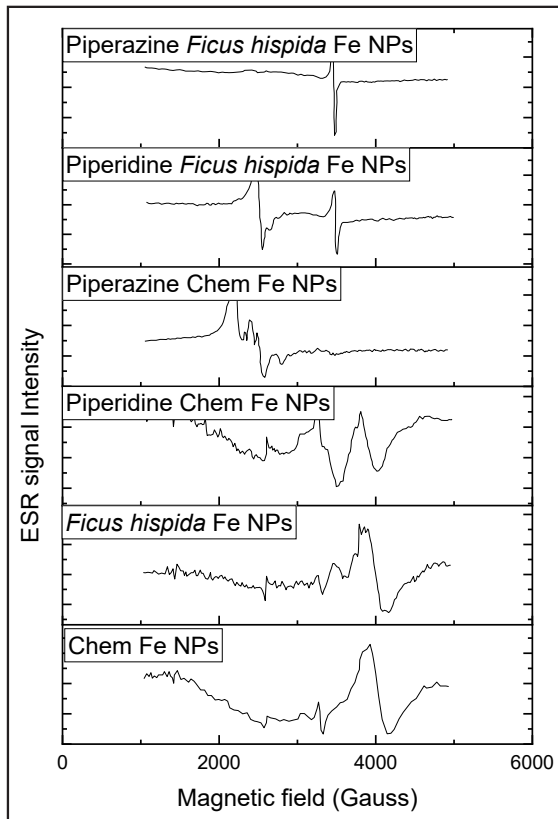
1289

Fig. 7. ESR spectrum of the different Fe NPs.

ESR measurements were taken from 1000G to 5000G. The spectrum was single and broad line centered at around 4000G for chemically synthesized Fe NPs and *Ficus hispida* synthesized Fe NPs. A slight shift towards the left side was observed on comparing the spectrum of *Ficus hispida* synthesized Fe NPs to chemically synthesized Fe NPs (38). On immobilizing the chemically synthesized Fe NPs using piperidine, a higher spectrum and a lower intensity spectrum was observed around 3300G and 3900G. On using piperazine for immobilizing chemically synthesized Fe NPs a rather heavy shift was observed with a narrower peak near 2200G. On immobilizing *Ficushispida* synthesized Fe NPs using piperidine, two peaks were identified near 2700G and 3900G. on immobilizing *Ficus hispida* synthesized Fe NPs using piperazine, a very narrow peak was identified near 3700G.

Degradation efficiency and residual antibiotic activity

The degradation efficiency was identified for both sets of experiments conducted without the presence of sunlight and with the presence of sunlight. For all experiments, degradation of neomycin rich antibiotic waste water was consistently better under simulated sunlight, compared to the degradation experiments conducted without the presence of sunlight. Effect of piperdine and piperamine immobilization was significant only under the presence of

Table 1. Degradation efficiency and residual antibacterial activity

NPs type used for degradation Experiments	Surface area (m²/g)	Absence of sunlight		Under sunlight	
		Degradation η%	Inhibition zone (cm)	Degradation η%	Inhibition zone (cm)
Chem Fe NPs	4.8	61.39	11.37	69.32	10.96
Ficus hispida Fe NPs	6.3	69.61	10.86	79.84	12.24
Piperidine immobilized Chem Fe NPs	4.91	61.84	11.21	86.32	14.12
Piperazine immobilized Chem Fe NPs	4.96	69.11	10.41	88.41	14.64
Piperidine immobilized *Ficus hispida* Fe NPs	6.41	62.13	10.09	91.32	15.12
Piperazine immobilized *Ficus hispida* Fe NPs	6.52	68.32	9.87	90.12	14.98

Photocatalytic degradation of (neomycin) antibiotic concentrated pharmaceutical disposals using *Ficus hispida* synthesized fe nanoparticels under simulated sunlight

photo-catalysis [53].The degradation efficiency of the Fe NPs under simulated sunlight and in the absence of sunlight is shown in Table 1. On conducting residual antibacterial activity experiments using clostridium bacteria, the variations in inhibition zone was identified after 15 min degradation, for different Fe NPs reactions. The variations in the inhibition zone were recorded and indicated in Table 1.

Conclusion

In this study, we investigated the degradation of neomycin antibiotic-rich pharmaceutical wastewater using Fe nanoparticles (NPs) synthesized through biosynthesis with *Ficus hispida* and chemical synthesis with sodium borohydride. The Fe NPs were immobilized using piperidine and piperazine and tested under photocatalytic conditions. Results showed that piperazine-immobilized *Ficus hispida* Fe NPs had the highest degradation efficiency (90.12%) compared to other tested NPs. A linear relationship comparable to the Langmuir-Hinshelwood model was established, indicating that adsorption equilibrium was maintained throughout the photocatalytic degradation process. These findings suggest that this approach may be a viable option for degrading toxins in pharmaceutical wastes.

References

1. Richter, A.P., Brown, J.S., Bharti, B. et al. (2015) An environmentally benign antimicrobial nanoparticle based on a silver-infused lignin core. Nat Nanotechnol, 10(9), 817-823.

2. Terry, T. (2022) The Antibacterial and Antibiotic Potentiating Activity of Marine Sponge *Ircinia fusca* Against Fish Pathogens. Curr Trends Biotechnol Pharm, 16(1) 133–140.

3. Mramba, A.S., Ndibewu, P.P., Sibali, L.L. & Makgopa, K. (2020) A review on electrochemical degradation and biopolymer adsorption treatments for toxic compounds in pharmaceutical effluents. Electroanalysis, 32(12), 2615-2634.

4. Lenart-Boroń, A., Prajsnar, J. & Boroń, P. (2017) Survival and antibiotic resistance of bacteria in artificial snow produced from contaminated water. Water Environ Res, 89(12), 2059-2069.

5. Bhatt, E., & Gauba, P. (2021) A Sustainable approach for Phytoremediation of Amoxicillin using Ocimumbasilicum. Curr Trends Biotechnol Pharm, 15(4), 426–435.

6. Nair, S., Kwatra, N., & Abraham, J. (2022) Isolation and Characterization of Biofilm Producing Bacteria from Water Treatment Tank. Curr Trends Biotechnol Pharm, 15(6), 34–39.

7. Wang, J. & Chen, H., (2020) Catalytic ozonation for water and wastewater treatment: recent advances and perspective. Sci Total Environ, 70(1), 135249.

8. Wenjun, L.I., Di, W.U., Xin, S.H.I., et al. (2012) Removal of organic matter and ammonia nitrogen in azodicarbonamide wastewater by a combination of power ultrasound radiation and hydrogen peroxide. Chin J Chem Eng 20(4), 754-759.

9. Martínez-Huitle, C.A. & Panizza, M., (2018) Electrochemical oxidation of organic pollutants for wastewater treatment. Curr Opin Electrochem, 11(1), 62-71.

10. Prathima, G. (2023) Environmental Bioremediation of DDT-Contaminated Soil by Using the Mushroom Extract of L. edodes. Curr Trends Biotechnol Pharm, 17(1), 603-608.

11. Umar, M. & Aziz, H.A., (2013) Photocatalytic degradation of organic pollutants in water. (Ed) Rashed M N, In Organic pollutants-monitoring, risk and treatment. pp. 195-208.

Current Trends in Biotechnology and Pharmacy
Vol. 17(Supplementary issue - 3B) 1278-1292,September 2023, ISSN 0973-8916 (Print), 2230-7303 (Online)
10.5530/ctbp.2023.3s.63

1291

12. Elias, M., Uddin, M.N., Hossain, M.A., et al. (2019) An experimental and theoretical study of the effect of Ce doping in ZnO/CNT composite thin film with enhanced visible light photo-catalysis. Int J Hydrog Energy, 44(36), 20068-20078.

13. Loh, J.Y., Sharma, G., Kherani, N.P. & Ozin, G.A., (2021) Post-Illumination Photoconductivity Enables Extension of Photo-Catalysis after Sunset. Adv Energy Mater, 11(41), 2101566.

14. Wang, D. & Chen, Y. (2016) Critical review of the influences of nanoparticles on biological wastewater treatment and sludge digestion. Crit Rev Biotechnol, 36(5), 816-828.

15. Aragaw, T.A., Bogale, F.M. &Aragaw, B.A., (2021) Iron-based nanoparticles in wastewater treatment: A review on synthesis methods, applications, and removal mechanisms. J Saudi Chem Soc, 25(8), 101280.

16. Fowsiya, J., Madhumitha, G., Al-Dhabi, N.A. & Arasu, M.V., (2016) Photocatalytic degradation of Congo red using Carissa edulis extract capped zinc oxide nanoparticles. J Photochem Photobiol B Biol, 162(1), 395-401.

17. Luo, F., Chen, Z., Megharaj, M. and Naidu, R., (2014) Biomolecules in grape leaf extract involved in one-step synthesis of iron-based nanoparticles. RSC Adv, 4(96), 53467-53474.

18. Uzair, B., Liaqat, A., Iqbal, H., et al. (2020) Green and cost-effective synthesis of metallic nanoparticles by algae: Safe methods for translational medicine. J Bioeng, 7(4), 129–153.

19. Gunasekar, R., Goodyear, R. L., Silvestri, I. P., & Xiao, J. (2022) Recent developments in enantio-and diastereoselective hydrogenation of N-heteroaromatic compounds. Org Biomol Chem 20(9), 1794-1827.

20. Bolleddula, J., DeMent, K., Driscoll, J. P., et al. (2014) Biotransformation and bio-activation reactions of alicyclic amines in drug molecules. Drug Metab Rev, 46(3), 379-419.

21. Aaltonen, N., Savinainen, J. R., Ribas, C. R., et al. (2013) Piperazine and piperidine triazole ureas as ultrapotent and highly selective inhibitors of monoacylglycerol lipase. Chem Biol 20(3), 379-390.

22. Tekle-Röttering, A., Jewell, K. S., Reisz, et al. (2016) Ozonation of piperidine, piperazine and morpholine: Kinetics, stoichiometry, product formation and mechanistic considerations. Water Res, 88(1), 960-971.

23. Mohamadpour, F. (2020) Green and convenient one-pot access to polyfunctionalized piperidine scaffolds via glutamic acid catalyzed Knoevenagel-intramolecular [4+2] aza-Diels-Alder imin-based multi-component reaction under ambient temperature. Polycycl Aromat Compd, 40(3), 681-692.

24. Paul, B., Vadivel, S., & Dhar, S. S. (2016) α-Fe2O3 immobilized benzimidazolium tribromide as novel magnetically retrievable catalyst for one-pot synthesis of highly functionalized piperidines. Chin Chem Lett, 27(11), 1725-1730.

25. Lotfian, N., Heravi, M. M., Mirzaei, M., & Heidari, B. (2019) Applications of inorganic-organic hybrid architectures based on polyoxometalates in catalyzed and photo-catalyzed chemical transformations. Appl Organomet Chem, 33(4), e4808.

26. Niknam, K., Deris, A., & Panahi, F. (2013) Silica-functionalized N-propylpiperazine for immobilization of palladium nanopar-

ticles as efficient heterogeneous catalyst for cyanation reactions. Chinese J Catal, 34(4), 718-722.

27. Neagoie, C., &Krchňák, V. (2012) Piperazine amide linker for cyclative cleavage from solid support: Traceless synthesis of dihydroquinoxalin-2-ones. ACS Comb Sci, 14(7), 399-402.

28. Liu, D., Chen, Y., Tran, T. T., & Zhang, G. (2021) Facile and rapid assembly of high-performance tannic acid thin-film nanofiltration membranes via Fe3+ intermediated regulation and coordination. Sep Purif Technol, 260(1), 118228.

29. Tomaszewska, E., Soliwoda, K., Kadziola, K., et al. (2013) Detection limits of DLS and UV-Vis spectroscopy in characterization of polydisperse nanoparticles colloids. J Nanomater, 60(1), 1-10.

30. Mehta, B.K., Chhajlani, M. & Shrivastava, B.D. (2017) Green synthesis of silver nanoparticles and their characterization by XRD. J Phys Conf Ser, 836(1), 1-4.

31. Radini, I.A., Hasan, N., Malik, M.A. & Khan, Z. (2018) Biosynthesis of iron nanoparticles using Trigonella foenum-graecum seed extract for photocatalytic methyl orange dye degradation and antibacterial applications. J Photochem Photobiol B Biol, 183(1):,154-163.

32. Shao, F., Zhou, S., Xu, J., et al. (2019) Detoxification of Cr (VI) using biochar-supported Cu/Fe bimetallic nanoparticles. Desalin Water Treat, 158(1), 121-129.

33. Sobhani, S., Ghasemzadeh, M.S. &Honarmand, M. (2014) Piperidine and piperazine immobilized on iron oxide nanoparticles as magnetically recyclable heterogeneous catalysts for one-pot synthesis of β-phosphonomalonates. Catal Letters, 144(9),1515-1523.

34. Hashemzadeh, M., Nilchi, A., Hassani, A. H., &Saberi, R. (2019) Synthesis of novel surface-modified hematite nanoparticles for the removal of cobalt-60 radiocations from aqueous solution. Int J Environ Sci Technol, 16(1), 775-792.

35. Jeevanandam, J., Chan, Y. S., & Danquah, M. K. (2016) Biosynthesis of metal and metal oxide nanoparticles. Chem Bio Eng Rev, 3(2), 55-67.

36. Huang, L., Luo, F., Chen, Z., Megharaj, M., & Naidu, R. (2015) Green synthesized conditions impacting on the reactivity of Fe NPs for the degradation of malachite green. Spectrochim Acta A, 137(1), 154-159.

37. Khan, M. S., Shah, J. A., Riaz, N., et al. (2021) Synthesis and characterization of Fe-TiO2 nanomaterial: performance evaluation for RB5 decolorization and in vitro antibacterial studies. J Nanomater, 11(2), 436-455.

38. Chen, M., Yao, J., Huang, Y., Gong, H., & Chu, W. (2018) Enhanced photocatalytic degradation of ciprofloxacin over Bi_2O_3/(BiO) $2CO_3$ heterojunctions: efficiency, kinetics, pathways, mechanisms and toxicity evaluation. J Chem Eng, 334(1), 453-461.